Construction and Building Materials 313 (2021) 125294

Contents lists available at ScienceDirect

Construction and Building Materials

journal homepage: www.elsevier.com/locate/conbuildmat

Experimental setup and numerical evaluation of the compression test on thin tiles for masonry timbrel vaults

Albert Cabané [a,*], Savvas Saloustros [a,b], Luca Pelà [a], Pere Roca [a]

[a] Department of Civil and Environmental Engineering, Universitat Politècnica de Catalunya (UPC-BarcelonaTech), Jordi Girona 1-3, 08034 Barcelona, Spain
[b] Laboratory of Earthquake Engineering and Structural Dynamics (EESD), School of Architecture, Civil and Environmental Engineering (ENAC), École Polytechnique Fédérale de Lausanne (EPFL), EPFL ENAC IIC EESD, GC B2 495, Station 18, 1015 Lausanne, Switzerland

ARTICLE INFO

Keywords:
Timbrel vaults
Thin clay tiles
Masonry
Compressive strength
Compressive test
Experimental tests
Historical buildings
Finite element analysis

ABSTRACT

Compressive tests on clay tiles used in historical masonry timbrel vaults are hindered by the relatively small thickness of the specimens, resulting in buckling or confinement problems depending on the loading direction. This paper presents an experimental campaign and a numerical validation of a novel testing setup for estimating the compressive strength of thin clay tiles used in timbrel vaults. The experimental campaign focuses on two different types corresponding to historical and modern handmade tiles. Experimental and numerical results show that the proposed test setup can be used for the estimation of the compressive strength of thin clay tiles.

1. Introduction

Timbrel vaults or timbrel arches are masonry elements made with thin clay tiles (with approximate dimensions 300 × 150 × 15/20 mm^3) and mortar (gypsum, lime or cement). The singularity of timbrel structures lies in their construction system. They are generally built with two or more layers of tiles placed with their bed tangent to the circumference of the vault or arch. The construction starts by fixing the first tiles to the walls at the sides of the vault using fast-setting mortar. Then, the first layer is developed through the gradual placement of tiles next to the previously placed ones. The use of fast-setting mortar makes possible a fast construction without scaffolding or supporting formwork. While the first layer is under construction, the following layer of tiles is built over the first one, using a mortar layer with a thickness of few millimetres between the two layers. Each successive layer is constructed adopting a head joint discontinuity with the previous one. This traditional construction technique is described in detail in works by A. Truñó [1], L. Moya [2] or R. Gulli [3]. The main characteristic of timbrel vaults and arches is their limited thickness, sometimes as small as 0.07 m, which is enabled by the use of the thin clay tiles. Another geometric characteristic is the high slenderness, intended as the ratio between the span and the thickness, reaching values even around one hundred [4]. This construction technique has been historically used to make vaults of a great variety of shapes and dimensions. The largest timbrel vault ever built is the dome over the crossing in St. John the Divine, New York, with a span of 33 m [5].

This construction system has been historically present in some littoral Mediterranean countries such as Spain ("*bóveda tabicada*" or "*volta a la catalana*"), France ("*voûte plate*" or "*voûte à la Roussillon*") and Italy ("*volta in foglio*"). The first architectural text that refers to the construction of the timbrel vaults, *Arte y Uso de la Arquitectura* [6], was written by Fray Lorenzo de San Nicolás in the 17th century and defines some stability rules relating the dimensions of the supporting wall to the length of the vault. In the middle of the 18th century, d'Espie [7] and A.

Abbreviations: t, thickness; t_t, thickness of the tile specimen; h_t, height of the tile specimen; w_t, width of the tile specimen; t_m, thickness of the mortar joint specimen; h_m, height of the mortar joint specimen; w_m, width of the mortar joint specimen; $f_{c,b}$, Normalized compressive strength of bricks; f_{bc}, Biaxial compressive strength; f_c, Uniaxial compressive strength; $f_{c\ TILE}$, Experimental compressive strength of tile specimen; $f_{c\ \mathrm{TILE,num}}$, Numerical compressive strength of tile specimen; f_m, Normalized compressive strength of mortar; E_b, Young's modulus of bricks; E_m, Young's modulus of mortar; ν, Poisson's ratio of bricks; $f_{t,b}$, Tensile strength of bricks; $f_{flex,m}$, Flexural strength of mortar; ρ_{nu}, Net dry density of bricks; ρ_{gu}, Gross dry density of bricks; W_s, Water absorption of bricks; CV, Coefficient of variation; ε, Strain; Gf_t, Tensile fracture energy; Gf_c, Compressive fracture energy.

* Corresponding author.
E-mail addresses: albert.cabane@upc.edu (A. Cabané), savvas.saloustros@epfl.ch (S. Saloustros), luca.pela@upc.edu (L. Pelà), pere.roca.fabregat@upc.edu (P. Roca).

https://doi.org/10.1016/j.conbuildmat.2021.125294
Received 18 June 2021; Received in revised form 28 September 2021; Accepted 16 October 2021
Available online 11 November 2021

Fig. 1. Example of two buildings with timbrel vaults using thin clay tile. A) R. Guastavino standing on a timbrel arch with the timbrel vaults under construction [Photograph adapted from [31], distributed under a CC BY 2.0 license]. B) Weaving room in Can Batlló industry in Barcelona at the beginning of the 20th century [Photograph by [32], AGDB. Diputació de Barcelona ©].

Laugier [8] described the construction system of the timbrel vault making special mention to its lightness and its incombustibility. In all of them, until well into the 19th century, the proportion rule was the main form for the design of these vaulted structures [9]. During the following 18th and 19th centuries the development of the scientific theory of the vaulted structures begins based on an equilibrium analysis and using graphical methods for the definition of the line of thrust within the arch. In this context, at the end of the 19th century, A. Gaudí [10,11] used funicular models in his constructions, and in 1892 R. Guastavino Moreno [12] executed strength tests in tension, bending and shear of some specimens to understand the structural behaviour of the timbrel vaults, classified as "cohesive constructions" (Fig. 1a).

The structural analysis of timbrel vaults between the end of the 19th century until today is characterized in general by two approaches. On the one hand, the assumption of a zero tensile strength of masonry motivated the use of equilibrium analysis, such as the membrane theory for domes developed by Rankine and popularized by Dunn [13]. In the middle of the 20th century, the equilibrium approach and the development of the fundamental theorems of plasticity were applied to masonry vaults in Heyman's limit analysis theories [14,15]. On the other hand, the application of Navier's elastic theory was applied to study the equilibrium of timbrel vaults based on the concepts of material strength and the principles of mechanics considering a homogeneous and isotropic material. Towards the end of the 20th century and until today, the Finite Element Analysis has been widely adopted as way to model vaulted structures [16]. The main challenge in this approach is the need for a detailed knowledge of the material properties, which for the case of existing timbrel vaults, is still a challenge due to the limited thickness of the utilized tiles and mortar joints.

The timbrel arches and vaults are present in traditional [17,18], industrial [19] (Fig. 1b) and vernacular [20] architecture. During the last century, R. Guastavino Expósito, the GATCPAC ("Grup d'Arquitectes i Tècnics Catalans per al Progrés de l'Arquitectura Contemporània", Group of Catalan Architects and Technicians for the progress of modern architecture), Le Corbusier [21], L. Moya [2,22], E. Dieste [23], and many others designed architectural structures based on this constructive system. Nowadays, the importance of the conservation and restoration of this type of masonry construction, considering not only its architectural value but also its structural authenticity [24], motivates the use of accurate analysis methods. Such tools are strongly necessary to estimate the strength capacity, their safety level against exceptional actions such as earthquakes, and the effect of possible changes in the use requiring a load increase. Furthermore, these structures have begun to play an important role in the 21st century architecture [25,26] thanks to the development of new computerized methods by P. Block et al. [27,28] allowing the design of innovative structures with great geometric versatility [29,30].

Modern structural analysis techniques for the design of new vaults or the structural assessment of existing ones, based either on FEM or other analytical approaches, require the knowledge of the materials' properties and in particular of the compressive strength of the vault's components. The compressive strength of the mortar from existing timbrel vaults can be obtained by the Double Penetration Test following the DIN 18555–9 [33–35]. With regard to the compressive strength of the units, the European EN 772–1 + A1:2016 [36] or the American ASTM C67-18 [37] are the main related standards, but present some limitations as for their applicability to thin tiles. EN 772–1 + A1:2016 considers testing the brick specimens flatwise with thicknesses over 40 mm for the determination of compressive strength. ASTM C67-18 allows testing the bricks specimens flatwise, that is, with the load applied in the same direction of the depth of the unit, considering half unit. The same standard also allows testing structural clay tile specimens in a position "such that the load is applied in the same direction as in service".

It becomes apparent that testing an entire thin tile unit flatwise or edgewise presents important drawbacks. Flatwise test configuration produces an overestimated strength due to the excessive confinement exerted by the loading platens to the small thickness specimen, while the edgewise test configuration may lead to an underestimated strength due to the geometrical effects provided by the excessive slenderness of the specimen [38]. Previous researches focused on tests on whole tiles applying the load perpendicular to the stretcher or header with a considerable specimen slenderness [39–43]. Testing a single tile perpendicular to the stretcher, the slenderness is around 7.5, and testing perpendicular to the header, the slenderness is around 15. This slenderness value is excessive for a compression test as the maximum capacity may be influenced by buckling of the specimens. To the authors' knowledge, no other recommendations are available in the literature.

This paper proposes a new methodology for testing thin clay tiles that overcomes the problems arising from their limited thickness, i.e. increased confinement or slenderness depending on the loading direction. For this purpose, a new test specimen assembled by two clay tiles is proposed. Considering the fact that tiles experience compression perpendicular to the stretcher and/or header direction within a timbrel vault, as well as the anisotropy of some types of clay units [44–46], the loading direction of the proposed specimen is perpendicular to the stretchers or headers of the tiles. The test on an assembled specimen instead of a single tile permits the reduction of the slenderness until values similar to those recommended by standards EN 772–1 + A1:2016 (0.4 to 3.84) or by the available literature on clay units (2.0 to 2.5) [47] or concrete units (1.5 to 4) [48,49].

The validation of the proposed testing setup for the characterization of the compressive strength of thin tiles is carried out through an experimental and numerical study. An experimental campaign was carried out on existing tiles extracted from timbrel vaults of two 19th century industrial buildings in Barcelona (Spain), one of them with an extension built at the beginning of the 20th century, as well as on modern handmade bricks with known mechanical characteristics. The latter case study allowed the comparison of the experimental results obtained from the new developed specimens with those derived from the standardized specimens. This research pays special attention to the use

of a new type of specimen and a test protocol for the strength characterisation of thin tiles with the following specific objectives: (1) Exploring the possibility of evaluating the mechanical behaviour of the tile under compression by means of laboratory tests; (2) analysing the consistency and reliability of the results obtained, as well as the acceptability of the experimental scattering; (3) determining size-effect correlations in the estimation of the compressive strength based on the comparison between experimental results and Finite Element simulations.

The paper is structured in five sections. After this introduction, Section 2 presents the experimental campaign performed on thin-tile units, including the description of the material, the specimen preparation, the test procedure and the experimental results. Section 3 presents the Finite Element (FE) simulation of the compression tests on thin clay tiles. Section 4 analyses the influence of the specimen geometry comparing the experimental and numerical simulation strength on modern handmade units. The paper ends with Section 5 presenting some concluding remarks.

2. Experimental study

This section presents the experimental campaign on historical thin-tiles and modern handmade bricks for determining their compressive strength. Details are provided related with the description of the materials, the preparation of the proposed specimen and its geometry, the testing setup and the experimental results. As mentioned, the historical samples were collected from two 19th century industrial buildings in Barcelona and the early 20th century building extension. All experimental tests were carried out at the Laboratory of Technology of Structures and Materials of the Technical University of Catalonia (UPC-BarcelonaTech).

2.1. Materials

In this work, two types of solid clay units were studied (Fig. 2). The first type of units corresponds to modern handmade solid clay bricks identified with the acronym 'Mo'. The second type of units corresponds to historical thin-tiles collected from three different timbrel vaults of two industrial buildings in Barcelona (Spain) and are identified with the acronyms 'Hi/I'. Both types, 'Mo' and 'Hi/I', were traditionally manufactured in a brickyard by moulding. They were shaped in a wooden mould sprinkled with dry fine sand and, after extracted from the mould, the bricks were fired into a coal-fired kiln. The number of the tested historical thin-tiles (Hi/I) was limited due to the restrictions imposed by the cultural value of the surveyed buildings, while the modern handmade (Mo) gave the possibility to test a larger number of specimens.

Table 1 presents a description of the sampled materials in terms of origin, acronym, number of tested specimens and average dimensions measured according to EN 772–16 [50]. With regard to the modern handmade units 'Mo', half of them were tested keeping their original thickness (Mo_1), while for the other half (Mo_2) their thickness was reduced to approximately 30 mm through polishing of the bed surfaces by a grinder fitted with a rotary diamond-impregnated disc.

The modern handmade bricks (Mo) have dimensions of 306 × 146 × 45.7 mm^3, which allowed their mechanical characterization in the laboratory following the EN 772–1 + A1:2016 [36]. Cut specimens with size 100 × 100 × 40 mm^3 were tested under compression and the result was corrected by considering the corresponding shape factor of 0.7 indicated by the standard to account for the confinement effect. The net and gross dry density were obtained according to EN 772–13 [51] and EN 772–3 [52], and the water absorption following EN 772–21 [53]. The values of Young's Modulus and Poisson's ratio were determined following the testing procedures proposed in [54], while the tensile strength was measured through uniaxial tensile tests [55]. Table 2 presents the mechanical characteristics of the modern handmade bricks (Mo).

2.2. Preparation of specimens and testing procedure

The motivation behind the proposal of a new test setup for the derivation of the compressive strength from thin clay tiles lies on their slender geometry. In particular, the small thickness of the tiles used in

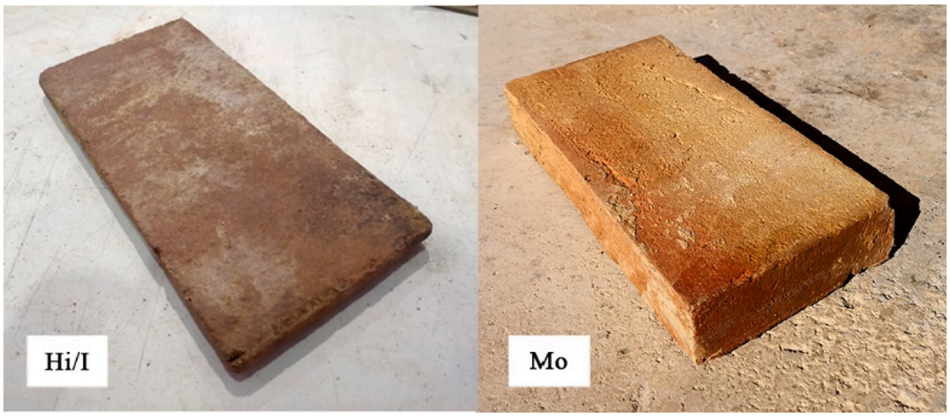

Fig. 2. Historical solid clay tile from industrial building (Hi/I) (left) and modern handmade solid clay brick (Mo) (right).

Table 1
Sampled materials in terms of origin, acronym, number of specimens collected and average dimensions. Values in brackets correspond to the Coefficients of Variation.

Sampled materials			
Origin	Acronym	Number of tiles	Av. Dimensions (mm) [Coefficient of Variation %]
Modern Handmade	Mo_1	6	306[1.4%] × 146[1.5%] × 45.7[2.7%]
	Mo_2	6	306[1.4%] × 146[1.5%] × 30.1[5.9%]
1878 building	Hi/I_1	7	294[0.4%] × 145[0.8%] × 20.8[2.6%]
Early 20th c. building	Hi/I_2	7	284[7.1%] × 145[1.0%] × 18.4[2.8%]
1870/75 building	Hi/I_3	6	299[1.3%] × 146[1.4%] × 20.0[4.1%]

Table 2
Mechanical characteristics of the modern handmade brick (Mo). Values in brackets correspond to the Coefficients of Variation.

	$f_{c,b}$ (MPa)	E_b (GPa)	ν (–)	$f_{t,b}$ (MPa)	ρ_{nu} (kg/m^3)	ρ_{gu} (kg/m^3)	W_s (%)
	EN 772–1	[54]	[54]	uniaxial test	EN 772–13	EN 772–13	EN 772–21
Modern Handmade	17.4 [8%]	5.55 [23%]	0.11 [51%]	1.4 [36%]	1631 [6%]	1761 [1%]	15.7 [7%]

timbrel vault construction (ranging between 15 mm and 20 mm) does not comply with the testing recommendations of EN 772–1 + A1:2016 [36] and ASTM C67-18 [37].

As an alternative to the testing of a single tile specimen, it is proposed here to test an assembled specimen consisting of two tile portions, bonded with a layer of cement mortar that is not in contact with the platens of the hydraulic press. The two specimens should be obtained from the same unit to reduce the variation in strength and stiffness between the two tiles. According to table A.1. of standard EN 772–1 + A1:2016, the height of the tested specimen can have any of the following values: 100 mm, 65 mm, 50 mm and 40 mm. Height values of 65 mm, 50 mm and 40 mm were discarded to reduce the effect of possible internal material imperfections that could increase the dispersion of the results. Fig. 3 presents the final geometry and composition of the proposed specimen, consisting of two portions of the same tile measuring 100 × 100 × t_t mm^3 each of them, bonded with an intermediate cement mortar joint with a thickness of 20 mm. The central cement mortar joint ensures an efficient coupling of the two tile portions, allowing the load transfer on both of them during the compressive test.

The extraction of the historical tiles from the vault was carefully carried out in situ with a chisel and a hammer, as shown in Fig. 4. First, was used a jackhammer to remove the pavement or the plaster and one tile was broken and removed with hammer and chisel. Then, a thin chisel was used to remove all the lime mortar joints around the tile to be extracted. Finally, a trapezoidal trowel was slowly inserted under the bed of the tile from the stretcher side and used as a lever. While levering the tile up, the trowel was lightly tapped with a nylon hammer, trying to avoid any crack appearance in the tiles. The tiles Hi/I$_3$ were extracted from the intrados of the vault after the removal of the plaster, while the Hi/I$_1$ and Hi/I$_2$ samples were extracted from the extrados of the vaults after the removal of the pavement. All mortar remains on the surface of the extracted tiles were manually removed using a wire brush with metal bristles without damaging the ceramic unit. Finally, the tiles were packaged, labelled and transported to the laboratory.

The proposed specimens were assembled in the laboratory according to the procedures specified in European Standards EN 772–1 + A1:2016 for solid clay units and the EN 998–2 [56] for cement mortar. Each tile was divided into two portions of 100 × 110 × t mm^3 (width × height × thickness) using a table saw equipped with a water jet (Fig. 5a). After the tile portions were saturated with water, they were connected with a fast-setting cement mortar layer using a mould specially developed for this test (Fig. 5b). This cement mortar layer with dimensions 100 × 80 × 20 mm^3 (width × height × thickness) was centred at the middle height of the two tiles. It is noted that the mortar does not reach the upper and lower boundaries of the tiles and thus it is not in contact with the hydraulic press platens. As a result, the mortar does not carry the load during the test and acts only as a coupling device between the two tiles. The compressive strength (f_m) and the bending strength ($f_{flex,m}$) of the binding mortar were evaluated according to EN 1015–11 [57], by using prisms with dimensions of 160 × 40 × 40 mm^3 that were casted with the same material employed by the mason during the construction of the assembled specimens. The evaluation of the Young's modulus (E_m) was carried out on mortar prismatic specimens of 160 × 40 × 40 mm^3 according to the testing procedures proposed in [54]. A summary of the results is presented in Table 3. After 24 h of the mortar casting, the assembled specimen was removed from the mould and was left to dry in a laboratory environment for a minimum of 14 days at a temperature above 15 °C and a relative humidity below 65%. Lastly, the load surfaces of the assembled specimen were dry-polished by a 3-axis vertical milling machine fitted with a rotary diamond disc to reduce with high precision the height from 110 mm to 100 mm (Fig. 5c). This aimed to guarantee that the loading surfaces were smooth and on the same plane, avoiding any possible source of imperfection on the loading planes. Finally, 29 specimens were obtained, 12 of modern handmade brick (6 Mo$_1$ and 6 Mo$_2$) and 17 of historical tiles (5 Hi/I$_1$, 7 Hi/I$_2$ and 5 Hi/I$_3$).

The assembled specimens were tested making use of an Ibertest testing machine composed by a steel frame with a load cell of 200 kN (AUTOTEST 200/10 SW) and connected to a MD5 electronic module for data acquisition. The assembled specimens were centred on the steel plates with the grinded surfaces orthogonal to the direction of the loading, and tested under displacement control at a rate of 0.2 mm/min (Fig. 5d). The rate of 0.2 mm/min was calibrated empirically in order to guarantee, at least, a test duration of 60 s. The tests were stopped manually after registering part of the post-peak softening response.

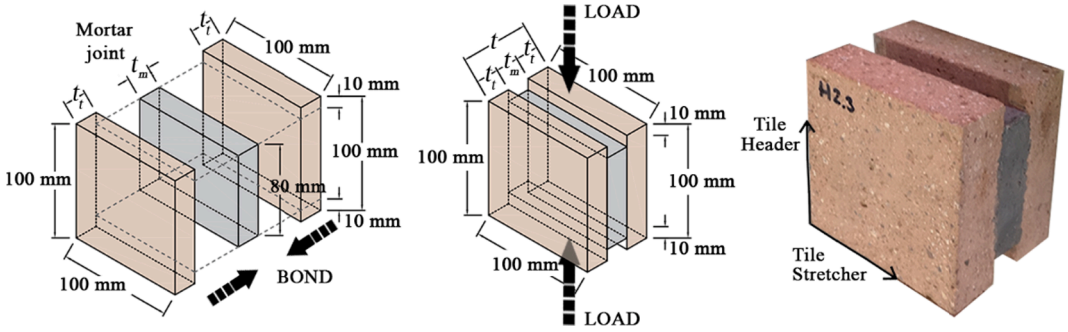

Fig. 3. Specimen proposed to obtain the compressive strength of the tile: specimen components (left), loading direction considered over the specimen (centre), and photography of Mo$_2$ specimen (right).

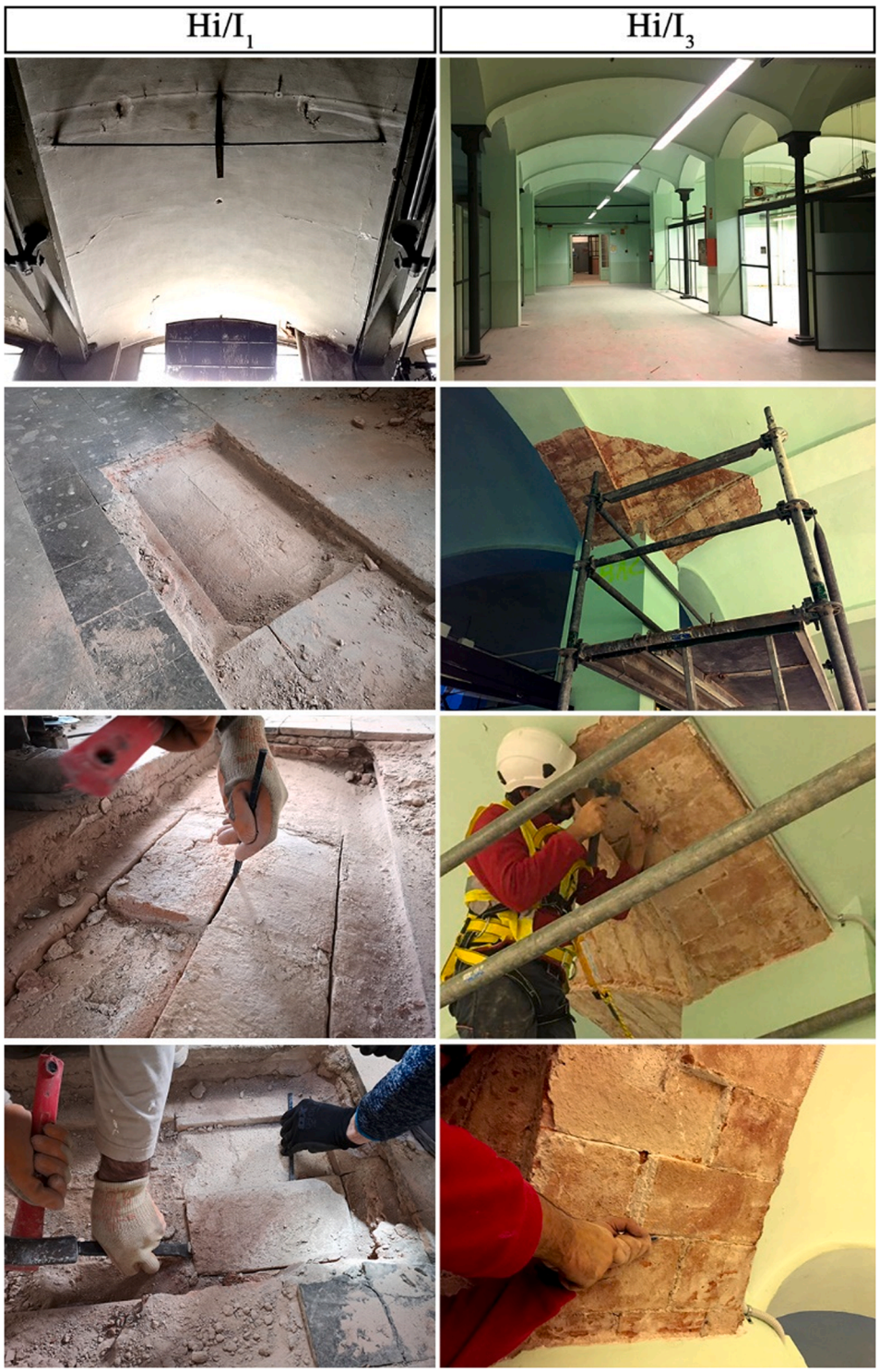

Fig. 4. The extraction process of the historical tiles from the existing vaults in two different buildings. The left column shows the extraction of Hi/I_1 samples from the extrados of the timbrel vault, and the right column shows the extraction of Hi/I_3 ones from the intrados of the timbrel vault.

2.3. Experimental results

Table 4 presents the thickness and the slenderness of the tiles used in each tested specimen, the slenderness of the specimen and the average compressive strength ($f_{c\ TILE}$) with the coefficients of variations. Table 4 also reports the ratio between the standardized strength of the standard specimen ($f_{c,b}$) and the experimental compressive strength of the developed specimens Mo_1 and Mo_2 ($f_{c\ TILE}$). The slenderness of the assembled specimen is defined as the ratio between the height and the total width of the specimen, considering as the total width the distance between the external faces of the specimen (i.e. the thickness of the two tiles plus the thickness of the cement mortar joint). The compressive strength of the tested specimens ($f_{c\ TILE}$) was calculated by dividing the maximum compressive load by the cross-sectional area of both tiles, without considering the area of the mortar layer. The displacement during the test was measured with the transducer from the actuator.

The coefficients of variation for the assembled specimens range between 20% and 34% and 11%-18% for historical and modern tiles,

Fig. 5. Manufacturing process of the proposed specimen. A) Tile portions with dimensions of 100 × 110 × t mm^3 obtained by cutting the tiles. B) Mould used to connect the two tiles together with a fast setting cement mortar. C) Dry polishing with a 3-axis vertical milling machine fitted with a rotary diamond disc of the assembled specimen. D) Assembled specimen tested in a hydraulic press.

Table 3
Mechanical characteristics of the binding mortar. Values in brackets correspond to the Coefficients of Variation.

	f_m (MPa)	$f_{flex,m}$ (MPa)	E_m (GPa)
	EN 1015–11	EN 1015–11	[54]
Mortar	61.4 [28%]	7.6 [22%]	34.2 [31%]

respectively. The higher variation in historical tiles is due to the larger inhomogeneity of the tiles as well as their non-industrialised manufacturing. However, the historical tiles Hi/I_1 and Hi/I_2, extracted from the same building, exhibited higher average strength than the modern ones due to the higher quality of the material. The assembled modern handmade specimens, Mo_1 and Mo_2, have close experimental compressive strengths despite the difference of 38% in the slenderness. The ratio between the standardized strength of the single tiles Mo_1 and Mo_2 and the compressive strength of the respective assembled specimens is 1.08 and 1.10 respectively. The geometrical influence of the specimens' configuration and the correlation with the standardized strength is presented in the section 4.

Fig. 6 shows the stress-displacement curves obtained during the uniaxial compressive load test of the assembled tile specimens. The stresses acting on the samples were computed as the ratio between the applied load and the area including the cross sections of both the tiles. The use of the displacement readings from the actuator result in an initial part with increasing stiffness in all stress–displacement curves. This behaviour is related with the adjustment of the platens to the faces of the tiles. After this, all curves present an approximately initial linear branch up to the maximum compressive strength. Just before the maximum load, the curves of the Mo_1_1, Mo_1_4, Mo_2_1 and Mo_2_3specimens presented a slight stress drop with subsequent increase up to the strength value. This point usually corresponds to the failure of the interface between the mortar and tile. Once the maximum load was reached, a brittle softening response followed with decreasing stress under increasing strain. The Hi/I specimens presented a more fragile post-peak response with a sudden stress drop.

The observed failure modes developed in two phases. First, thin vertical cracks parallel to the load direction appeared at the upper and lower parts of the tiles which were in contact with the platens [Fig. 7a]. Then, as the load continued to increase, these cracks spread further producing an arch-shaped crack that split the tile into two parts [Fig. 7b]. These cracks went through the total width of the tile causing the complete separation of the outer part [Fig. 7c]. As previously mentioned, some specimens presented a sudden vertical crack between

Table 4
Thickness and slenderness of the tiles and the assembled specimens, average compressive strength of the tested specimens ($f_{c\ TILE}$), ratio between the normalized strength of the standard specimen ($f_{c,b}$) and the compressive strength of the developed specimen $f_{c,b}$ / $f_{c\ TILE}$. Values in brackets correspond to the Coefficients of Variation.

Tested Specimens						
		t_t (mm)	Tile Slenderness	Specimen Slenderness	$f_{c\ TILE}$ (MPa)	$f_{c,b}$ / $f_{c\ TILE}$
Mo_1	6	46.0 [3.2%]	2.18 [2.7%]	0.89 [2.4%]	16.1 [11%]	1.08
Mo_2	6	30.1 [5.9%]	3.32 [7.2%]	1.25 [5.9%]	15.8 [18%]	1.10
Hi/I_1	5	21.0 [2.4%]	4.88 [2.8%]	1.73 [2.7%]	22.8 [22%]	–
Hi/I_2	7	18.3 [3.1%]	5.53 [3.6%]	1.90 [3.4%]	22.2 [20%]	–
Hi/I_3	5	20.0 [5.3%]	5.08 [5.1%]	1.64 [4.1%]	15.3 [34%]	–

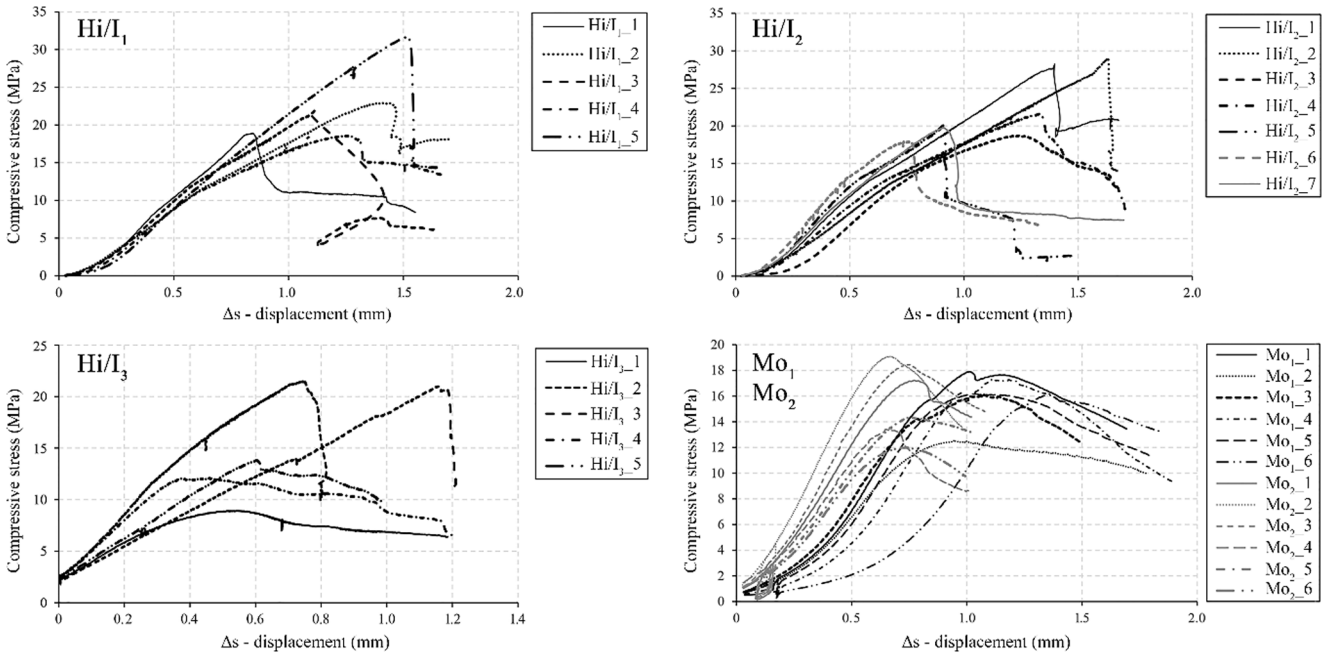

Fig. 6. The stress-displacement curves of the 29 assembled specimens under uniaxial compression.

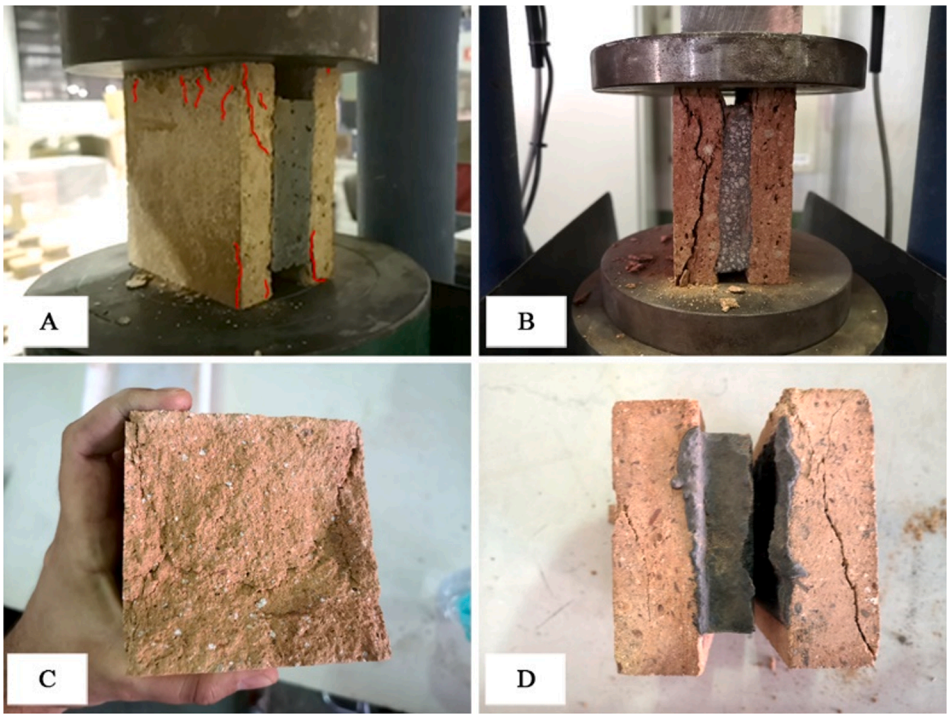

Fig. 7. The development of the failure mode during the test procedure. A) The surfaces of the specimen in contact with the platens develop small vertical cracks at the beginning of the loading. B) The arch-shaped crack developed through the width of each tile of the assembled specimen. C) Expulsion of the outer material after the crack has fully developed. D) Failure mechanism involving both a crack in the tile and a separation of the cement mortar and the tile.

the mortar joint and the tile, close to the maximum load capacity, which corresponded to a stress drop before the maximum capacity in their stress–strain relationship [Fig. 7d].

3. Numerical study

The proposed testing protocol was simulated using the Finite Element Method. The objective of the numerical analysis is to investigate the validity of the adopted experimental configuration for estimating the uniaxial compressive strength of thin clay tiles. Additionally, an insight is given on the influence of the thickness of the tiles and their mechanical properties, as well as the potential influence of the numerical parameters of the adopted modelling approach.

A continuum finite element approach was adopted with a distinct modelling of the tiles and the mortar. Fig. 8 presents the geometry and the used finite element mesh. The dimensions of the simulated clay tiles for the reference model were h_t = 100 mm (height), w_t = 100 mm (width), while different values for the thickness were considered (t_t = 20

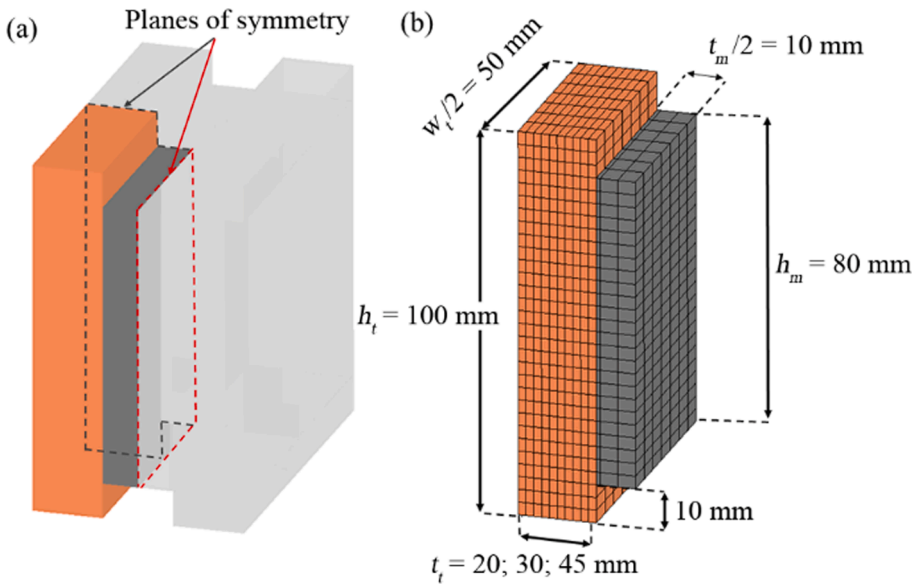

Fig. 8. (a) Specimen with the planes of symmetry (non-simulated part in grey), (b) Geometry of the reference model and finite element mesh.

mm; 30 mm; 45 mm). The dimensions of the binding mortar layer were $h_m = 80$ mm, $w_m = 100$ mm and $t_m = 20$ mm, as in the experimental campaign. Only a quarter of the specimen was modelled due to the symmetry along the two vertical middle planes (see Fig. 8). Isoparametric solid brick elements based on linear interpolation and $2 \times 2 \times 2$ Gauss integration were used for the mesh. The experiment was simulated by applying a vertical displacement at the top of the tile, restraining the vertical displacement at its base. The symmetry of the specimen was considered by restraining the displacements normal to the two planes of symmetry (see Fig. 8). The system of nonlinear equilibrium equations was solved using a secant method along with a line-search procedure. Convergence was achieved for a ratio between the norm of the iterative residual forces and the norm of the total external forces is lower than 10^{-2} (1%). Numerical simulations were performed with the finite element software COMET [58], while pre- and post-processing with GiD [59] developed at CIMNE, Barcelona.

Cracking and crushing of the units and the mortar was simulated using a continuum damage mechanics formulation with damage induced orthotropic behaviour along the principal stress axes. The model uses two distinct damage indices corresponding to tensile damage (i.e. cracking) and compressive one (i.e. crushing) [60]. This choice permits the differentiation between the nonlinear tensile and compressive behaviour. In particular, the tensile response is characterised by a linear branch up to the maximum strength, followed by an exponential softening branch. The compressive response is characterised by a parabolic hardening up to the maximum strength and a parabolic softening beyond it [61]. The failure criterion proposed by Lubliner et al. [62] was adopted in all simulations, with the modification introduced in [61] for controlling the shear behaviour. The above numerical strategy has been calibrated for the simulation of the compressive behaviour of masonry specimens in [63].

Table 5 presents the mechanical parameters for the tile and the mortar. The material properties for the tile correspond to those of the handmade solid clay tiles obtained in the experimental campaign presented in Section 2. The tensile fracture energy is calculated as Gf_t [J/m^2] $= 0.04 f_t^{0.7}$ (f_t in MPa) and the compressive fracture energy as Gf_c [J/m^2] $= 1.6 f_{c,b}$ ($f_{c,b}$ in MPa) [64]. The selected failure criterion needs the definition of the parameter ρ, which controls the triaxial compression, the ratio between biaxial and uniaxial compressive strength $f_{b,c} / f_c$ and the parameter κ that controls the shear response [61]. The first two parameters were calibrated through the simulation of the standardized experimental tests under compression of the Mo brick specimens with size $100 \times 100 \times 40$ mm^3 as described in Section 2.1. The parameter κ was defined equal to 0.16 as in [61,63] and its effect on the numerical results is investigated through a sensitivity analysis presented in Section 4. Linear elastic behaviour, with the Young's modulus corresponding to the experimentally obtained value, is adopted for the mortar as no damage was observed in it during the experimental campaign.

Fig. 9 presents the tensile damage of the specimen at the end of each analyses for the three studied thickness of $t_t = 20$ mm, 30 mm and 45 mm. All cases are characterized by initial cracking at the interface between mortar and brick and at the middle of the tile in proximity with the cement mortar (Fig. 10a). This crack propagates slowly during the analysis, while cracks start appearing at the top and bottom ends of the tile (Fig. 10b). These two cracks progress symmetrically towards the interior of the tile, and finally one of the two dominates and separates the tile into two parts (Fig. 10c). This crack corresponds to the delamination of the external part of the tile as observed in the experimental tests. Moreover, cracking exists as well in the mortar-tile interface, as was observed in some experimental tests.

Fig. 11 presents the vertical stress–strain graphs obtained from the numerical analyses. The curves resemble closely the experimental curves as obtained for the Hi/I and Mo specimens. The propagation of the crack that produces the separation of the tile into two parts results in the sudden drop of the capacity of the specimen for all cases and corresponds to the end of the analysis for the tile with a thickness of 30 mm. For the other two cases, the rest of the analysis is characterized by a plateau with crushing occurring at the bottom of the tile.

Table 5
Mechanical properties of tiles and the mortar used in the numerical simulations.

Property	Tiles	Mortar
E (GPa)	5.55	34.20
ν (–)	0.11	0.25
f_t(MPa)	1.4	–
f_c(MPa)	17.4	–
G_{ft}(J / m^2)	50	–
G_{fc}(J / m^2)	27,840	–
f_{bc}/f_c	1.15	–
ρ (–)	0.65	–

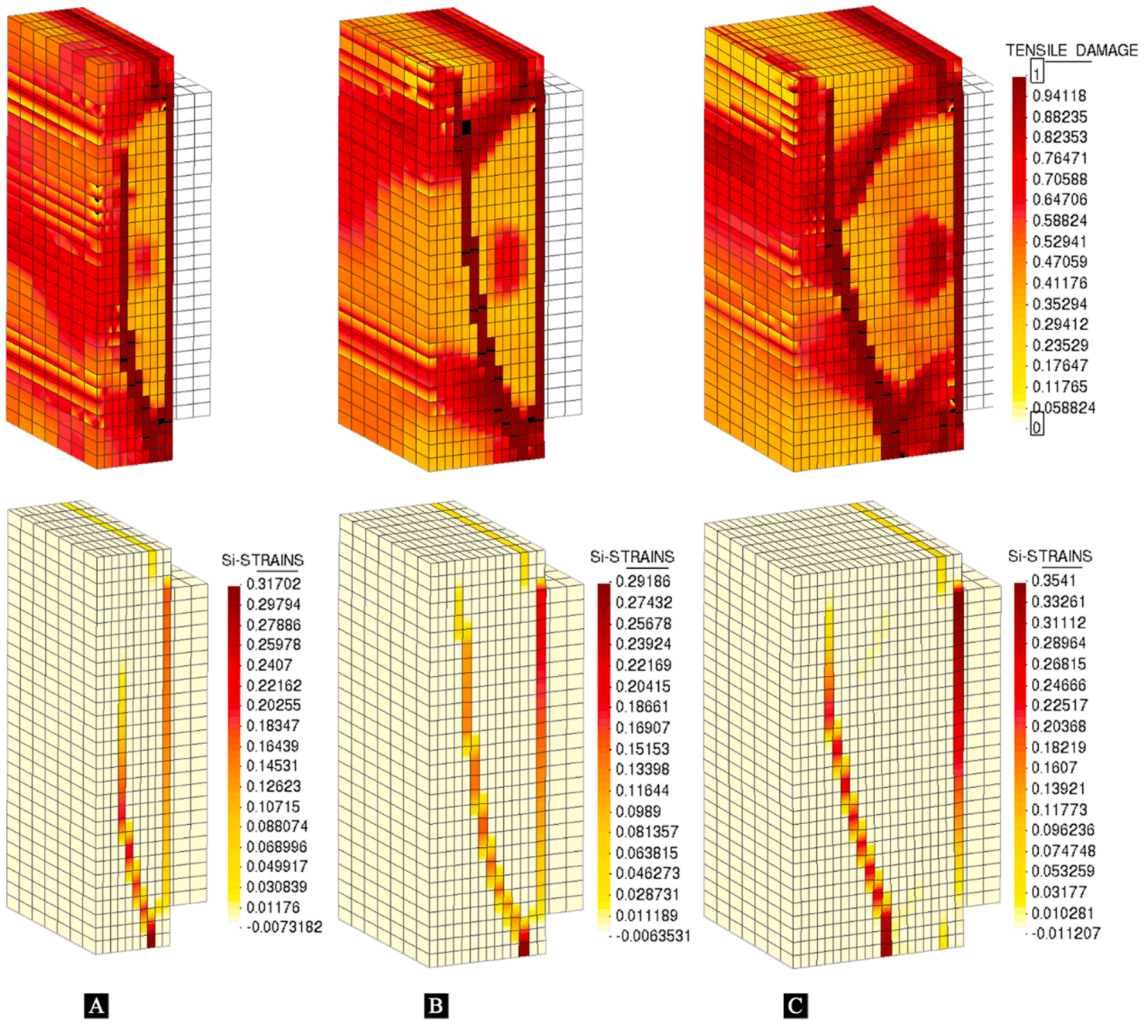

Fig. 9. Tensile damage (top) and maximum principal strains (bottom) contour for the analysis of a tile with thickness: (a) 20 mm, (b) 30 mm, and (c) 45 mm.

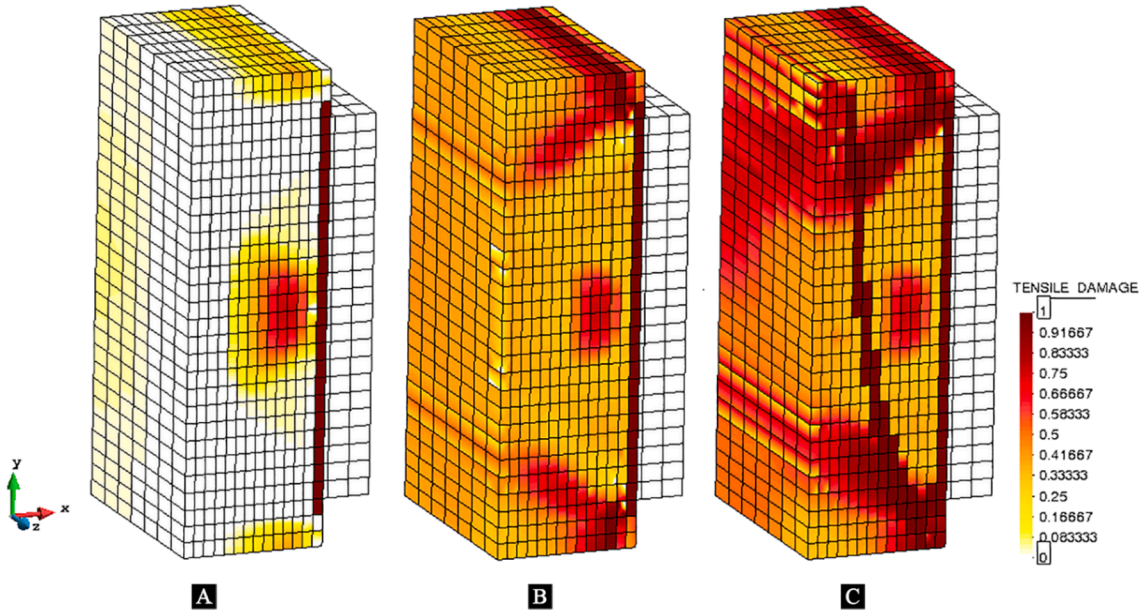

Fig. 10. Tensile damage of the simulated specimen with tile thickness 30 mm corresponding to a vertical displacement of: (a) 0.3 mm, (b) 0.45 mm and (c) 0.60 mm.

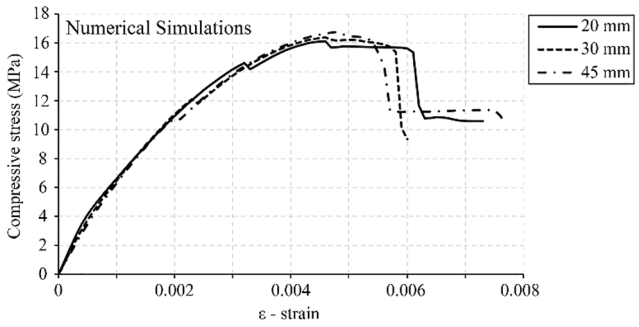

Fig. 11. Vertical strain against vertical stress for the three numerical simulations of the tiles with different thickness.

4. Discussion

The experimental campaign using the modern handmade bricks (Mo) allowed to obtain a correlation between the uniaxial compressive strength of a standardized single tile and that of the assembled specimen ($f_{c,b}$ / $f_{c\ TILE}$). As presented in Table 4 (Section 2) and Table 6, this ratio was 1.08 and 1.10 for a slenderness ratio of 0.89 (Mo_1 specimens with mean tile thickness of 46 mm) and 1.23 (Mo_2 specimens with mean tile thickness of 30 mm) respectively. The numerical analyses showed very similar results with $f_{c,b}$ / $f_{c\ TILE,num}$ = 1.04 for a slenderness ratio of 0.90 (tile thickness of 45 mm) and 1.06 for a slenderness ratio of 1.25 (tile thickness of 30 mm) (Table 6). These results were complemented with the numerical simulation of a specimen with a slenderness ratio 1.67 (tile thickness of 20 mm), resulting in $f_{c,b}$ / $f_{c\ TILE,num}$ = 1.08. The experimental and numerical results show that tests with the proposed specimen allow estimates of the uniaxial compressive strength of thin tiles that are slightly lower than the values given by standardized tests (between 5% and 10% lower). A correlation between the slenderness ratio and the $f_{c,b}$ / $f_{c\ TILE}$ seems to exist, with increasing slenderness resulting in lower values of the uniaxial compressive strength given by the proposed specimen.

The above results were further validated through a parametric numerical study. First, we investigated the influence of the parameter κ, controlling the shear response, which could not be calibrated through the experimental campaign. As described in [61], κ takes values between 0 and 1, with an increasing value resulting in a lower shear strength (for more information see [61 65]). The variation of κ between 0.0 and 0.3 changes slightly the $f_{c,b}$ / $f_{c\ TILE,num}$ without affecting the observed trend between slenderness and uniaxial strength prediction. As anticipated, a reduction in the value of κ for the same thickness results in a slight increase in the strength. The maximum change in the predicted compressive strength due to the variation of κ is approximately 7% for a tile with thickness of 45 mm. For the other two tile thickness, this variation drops to 5% and 3% for t_t = 30 mm and t_t = 20 mm, respectively. For all the cases, this parameter shows a marginal effect in the estimation of the compressive strength.

Next, the variation of the tensile strength and the tensile fracture energy was investigated. Three values were used for each one: ft = 1.0 MPa; 1.4 MPa; 1.8 MPa and G_{ft} = 25 J/m^2; 50 J/m^2; 75 J/m^2, with the middle values being the reference ones. The variation of these properties showed the same trend in the estimation of the compressive strength. For any tile thickness, lower values of the tensile strength or the fracture energy result in lower compressive strength and vice versa. The effect of these properties is anticipated as both of them are related with the cracking that appears within the specimen and drives the collapse mechanism in both experimental and numerical results. Lower tensile strength results in earlier cracking, while lower fracture energy to a more rapid crack propagation.

In overall, the results of the sensitivity analysis, presented in Table 6, show that $f_{c,b}$ / $f_{c\ TILE,num}$ lies for all the cases between 1.02 and 1.09. The results of the compressive fracture energy are omitted as this parameter does not influence the estimation of $f_{c,b}$ / $f_{c\ TILE,num}$. It is noted that the same failure mechanism has been obtained for all the cases, independently on the change of the material and numerical properties.

Table 6
Relationship between the compressive strength obtained from the numerical simulation of the proposed experiment ($f_{c\ TILE,num}$) with the uniaxial compressive strength of the tile ($f_{c,b}$).*Value for a tile thickness of 46 mm.

	Numerical $f_{c,b}$ / $f_{c\ TILE,num}$		
	t_t = 20 mm	t_t = 30 mm	t_t = 45 mm
κ = 0.0	1.05	1.04	1.02
κ = 0.16	**1.08**	**1.06**	**1.04**
κ = 0.3	1.12	1.09	1.09
ft = 1.0 MPa	1.13	1.09	1.08
***ft* = 1.4 MPa**	**1.08**	**1.06**	**1.04**
ft = 1.8 MPa	1.06	1.05	1.04
Gft = 25 J/m^2	1.09	1.07	1.05
G*ft* = 50 J/m^2	**1.08**	**1.06**	**1.04**
Gft = 75 J/m^2	1.07	1.06	1.08
Average Numerical	1.09	1.07	1.06
		$f_{c,b}$ / $f_{c\ TILE}$	
Experimental	–	1.10	1.08*

5. Conclusions

This paper has presented a test setup for the uniaxial compressive testing of thin clay tiles used in the construction of timbrel masonry vaults. The new test setup was validated through the combination of an experimental campaign on modern and historical handmade clay tiles extracted from two 19th century industrial buildings in Barcelona (Spain) and from the early 20th extension of one of them, and finite element simulations. The following conclusions can be drawn from the analysis of the experimental and numerical results:

- A relatively easy and efficient procedure was applied to extract the historical tiles from existing vaults. Common electric tool were employed, such as a jackhammer to remove the pavement or the plaster, together with manual chisel, a trapezoidal trowel and a nylon hammer for the careful extraction of the tiles from the existing vaults.
- The tests on assembled specimens allowed a reliable testing in compression of the tiles. The test on the proposed assembled specimen avoided the possible influence of instability effects induced by the excessive slenderness of the individual tiles. No tile buckling failure was observed in the experimental investigation.
- The failure mode of the tiles in both, experimental and numerical results, was characterized by the splitting of the tile into two parts due to the propagation of a crack throughout the whole width of the tile. In some cases, a debonding between the tile and the cement mortar was also observed.
- The experimental and numerical results show that the proposed test setup can estimate the uniaxial compressive strength of the tile with a difference between 5% and 10% from the one given by tests on standardized brick specimens.
- The numerical investigation showed that the change in the thickness, as well as the variation of the tensile and shear strength and the tensile fracture energy, have a marginal influence on the estimation of the uniaxial compressive strength by using the proposed setup. The ratio between the uniaxial tensile strength of a single brick (input data of the numerical model) and the uniaxial compressive strength computed using the proposed assembled specimen ranged between 1.02 and 1.09.
- Testing the thin tile using the proposed assembled specimen has proved to be an advantageous technique for the evaluation of the compressive strength of thin tile units. It is suggested to test at least a

set of six units extracted from an existing vault to obtain a reliable estimation of the compressive strength.

Future works could address the extension of the experimental database by including the application to a wider sample of tiles extracted from existing timbrel vaults.

CRediT authorship contribution statement

Albert Cabané: Conceptualization, Methodology, Validation, Formal analysis, Investigation, Resources, Data curation, Writing – original draft, Visualization. **Savvas Saloustros:** Conceptualization, Methodology, Software, Validation, Formal analysis, Investigation, Data curation, Writing – review & editing, Visualization. **Luca Pelà:** Conceptualization, Methodology, Validation, Investigation, Resources, Writing – review & editing, Supervision, Project administration, Funding acquisition. **Pere Roca:** Conceptualization, Methodology, Validation, Investigation, Resources, Writing – review & editing, Supervision, Project administration, Funding acquisition.

Declaration of Competing Interest

The authors declare that they have no known competing financial interests or personal relationships that could have appeared to influence the work reported in this paper.

Acknowledgements

The authors gratefully acknowledge the financial support from the Ministry of Science, Innovation and Universities of the Spanish Government (MCIU), the State Agency of Research (AEI) as well as that of the ERDF (European Regional Development Fund) through the project SEVERUS (Multilevel evaluation of seismic vulnerability and risk mitigation of masonry buildings in resilient historical urban centres, ref. Num. RTI2018-099589-B-I00). Support from MCIU through a predoctoral grant awarded to the first author is also gratefully acknowledged.

References

[1] Á. Truñó, Constucción de bóvedas tabicadas, Instituto Juan de Herrera (2004).
[2] L. Moya Blanco, *Bóvedas tabicadas*. Ministerio de la Gobernación Dirección General de Arquitectura Servicio de Publicaciones, 1947.
[3] R. Gulli, Arte y técnica de la construcción tabicada, in: Las bóvedas de Guastavino en América, Instituto Juan de Herrera, 1999, pp. 59–72.
[4] S. Huerta Fernández, Essays on the History of Mechanics, Birkhäuser Basel, Basel, 2003.
[5] N. Zawisny, C. Fivet, J. Ochsendorf, Guastavino design of the 1909 thin brick dome of the Cathedral of St John the Divine, Constr. Hist. 32 (2) (2017) 39–66, https://doi.org/10.2307/26476167.
[6] F. L. De San Nicolás, *Arte y uso de la arquitectura: con el primer libro de Euclides traducido en castellano: primera parte*. 1796.
[7] F.-F. d'Espié, *Manière de rendre toutes sortes d'édifices incombustibles, ou Traité sur la construction des voûtes, faites avec des briques et du plâtre, dites voûtes plates, et d'un toit de brique, sans charpente, appelé comble briqueté, de l'invention de M. le comte d.* 1754.
[8] M.-A. Laugier, *Essai sur l'architecture*. 1753.
[9] E. Martínez Redondo, "El proyecto de bóvedas tabicadas siguendo reglas de proporción," in *Actas del Décimo Congreso Nacional y Segundo Congreso Internacional Hispanoamericano de Historia de la Construcción*, 2017, vol. 3, pp. 1367–1380.
[10] J. L. González Moreno-navarro, "Configuración constructiva de las bóvedas «convexas» de la iglesia de la Colonia Güell, obra de Antonio Gaudí," in *Tercer Congreso Nacional de Historia de la Construcción, Sevilla*, 2000, pp. 431–441.
[11] J.M. Adell, A. García Santos, Gaudí y las bovedas de las escuelas de la Sagrada Familia, Inf. la Construcción 56 (496) (2005) 31–45, https://doi.org/10.3989/ic.2005.v57.i496.461.
[12] R. Guastavino, Essay on the Theory and History of Cohesive Construction, Applied Especially to the Timbrel Vault, J. Parkhill & . CO., Boston, 1893.
[13] W. Dunn, Notes on the stresses in framed spires and domes, J. R. Inst. Br. Archit. Third Ser. 11 (1904) 401–412.
[14] S. Huerta Fernández, "Mechanics of masonry vaults: The equilibrium approach," in: Historical Constructions 2001, Possibilities of numerical and experimental techniques. Proceedings of the 3rd International Seminar, P. Lourenço and P. Roca, Eds. Guimarães, 2001, pp. 47–70.
[15] J. Heyman, The stone skeleton, Int. J. Solids Struct. 2 (2) (Apr. 1966) 249–279, https://doi.org/10.1016/0020-7683(66)90018-7.
[16] P. Roca, M. Cervera, G. Gariup, L. Pelà, Structural analysis of masonry historical constructions. Classical and advanced approaches, Arch. Comput. Methods Eng. 17 (3) (2010) 299–325, https://doi.org/10.1007/s11831-010-9046-1.
[17] A. Paricio Casademunt, Secrets d'un sistema constructiu: l'Eixample, Edicions UPC (2001).
[18] J.G. de Churtichaga, Aspectos constructivos de la reconstruccion de Villanueva de la Cañada. El uso de los sistemas de bóvedas tabicadas y su perspectiva histórica, Conarquitectura 8 (2003) 81–93.
[19] R. Lacuesta, Catalan industrial architecture in the last quarter of the 19th century and first quarter of the 20th century, Catalan Hist. Rev. 75 (10) (2017) 59–75, https://doi.org/10.2436/20.1000.01.132.
[20] A. Feu i Jordana, Les voltes de rajola doblada: Construcció i seguretat estructural de les eglésies barroques catalanes, Universitat Politècnica de Catalunya (2017).
[21] R. Gulli, La memoria delle tecniche: Le Corbusier e la volta catalana, Clua edizioni (1994).
[22] J.M. Adell, A. Rolando, Luis Moya y las bóvedas tabicadas en la posguerra española, Inf. la Construcción 56 (496) (2005) 25–29, https://doi.org/10.3989/ic.2005.v57.i496.460.
[23] A.J. Mas Guindal, J.M. Adell, Eladio Dieste y la cerámica estructural en Uruguay, Inf. la Construcción 56 (496) (2005) 13–23, https://doi.org/10.3989/ic.2005.v57.i496.459.
[24] ICOMOS, "ICOMOS (2003) - ICOMOS Charter," Princ. Anal. Conserv. Struct. Restor. Archit. Herit., pp. 3–6, 2003.
[25] D. López, T. Van Mele, P. Block, La bóveda tabicada en el siglo XXI, Inf. la Construcción 68 (544) (2016) 162, https://doi.org/10.3989/ic.15.169.m15.
[26] P. Block, M. Rippmann, Das katalanische Gewölbe – Ein Konstruktionsprinzip mit Geschichte und Zukunft / The Catalan Vault – A Historical Structural Principle with a Bright Future, DETAIL 5 (2013) 528–536.
[27] P. Block, J. Ochsendorf, Thrust network analysis: a new methodology for three-dimensional equilibrium, J. Int. Assoc. Shell Spat. Struct. 48 (155) (2007) 167–173.
[28] M. Rippmann, L. Lachauer, P. Block, Interactive vault design, Int. J. Sp. Struct. 27 (4) (2012) 219–230, https://doi.org/10.1260/0266-3511.27.4.219.
[29] D. López López, M. Domènech Rodríguez, M. Palumbo Fernández, 'Brick-topia', the thin-tile vaulted pavilion, Case Stud. Struct. Eng. 2 (2014) 33–40, https://doi.org/10.1016/j.csse.2014.09.001.
[30] D. López, M. Domènech, J. Brazo, and P. Block, "Thin-tile vault for the Seventh World Urban Forum in Medellín," in: IASS-SLTE 2014 Symp., no. September 2014, 2014.
[31] E. F. Stevens, "Rafael Guastavino stands on recently laid tile arch along Boylston Street, construction of the McKim Building." 1889.
[32] C. Comas, "Sala de tissatges." 1907.
[33] Deutsche Norm, "DIN 18555-9 Testing of mortar containing mineral binders - Part 9: Determining the compressive strength of hardened mortar." 1999.
[34] L. Pelà, P. Roca, A. Aprile, Combined in-situ and laboratory minor destructive testing of historical mortars, Int. J. Archit. Herit. 12 (3) (2018) 334–349, https://doi.org/10.1080/15583058.2017.1323247.
[35] D. Marastoni, L. Pelà, A. Benedetti, P. Roca, Combining Brazilian Tests on masonry cores and Double Punch Tests for the mechanical characterization of historical mortars, Constr. Build. Mater. 112 (2015) 112–127, https://doi.org/10.1016/j.conbuildmat.2016.02.168.
[36] European Committee for Standardization (CEN), "EN 772-1+A1 Methods of test for Masonry Units - Part 1: Determination of Compressive Strength." 2016.
[37] American Society for Testing and Materials (ASTM), "C67-20 Standard Test Methods for Sampling and Testing Brick and Structural Clay Tile." 2020, doi: 10.1520/C0067_C0067M-20.
[38] V.J.G.M. Mier, Strain-softening of concrete under multiaxial loading conditions, Tech. Hogesch. Eindhoven (1984), https://doi.org/10.6100/IR145193.
[39] D.L. López, M.D. Rodríguez, Tile vaults. Structural analysis and experimentation / Voltes de maó de pla. Anàlisi estructural i experimentació / Bóvedas tabicadas, Análisis estructural y experimentación. (2015).
[40] D. López López, M. Doménech Rodríguez, and M. Palumbo Fernández, "Using a construction technique to understand it: thin-tile vaulting," in: SAHC2014 – 9th International Conference on Structural Analysis of Historical Constructions, Universidade do Minho, Ed. 2014.
[41] J. Llorens, M. Llorens, M.A. Chamorro, J. Gómez, C. Barris, Experimental study on the vertical interface of thin-tile masonry, Constr. Build. Mater. 261 (2020), 119976, https://doi.org/10.1016/j.conbuildmat.2020.119976.
[42] J. Llorens, M. Llorens, M.A. Chamorro, J. Soler, Experimental behavior of brick masonry under uniaxial compression on parallel-to-face brick. Single-leaf case study, Int. J. Archit. Herit. 14 (1) (2020) 23–37, https://doi.org/10.1080/15583058.2018.1503361.
[43] J. Llorens et al., "Experimental Behavior of Thin-Tile Masonry under Uniaxial Compression. Multi-Leaf Case Study," Materials (Basel)., 14(11), p. 2785, 2021, doi: 10.3390/ma14112785.
[44] A. Fódi, Effects influencing the compressive strength of a solid, fired clay brick, Period. Polytech. Civ. Eng. 55 (2) (2011) 117, https://doi.org/10.3311/pp.ci.2011-2.04.
[45] P.B. Lourenço, F.M. Fernandes, F. Castro, Handmade clay bricks: chemical, physical and mechanical properties, Int. J. Archit. Herit. 4 (1) (2010) 38–58, https://doi.org/10.1080/15583050902871092.
[46] P. Matysek, M. Witkowski, A comparative study on the compressive strength of bricks from different historical periods, Int. J. Archit. Herit. 10 (4) (2016) 396–405, https://doi.org/10.1080/15583058.2013.855838.

[47] J. Morton, M.D. Kotsovos, M.N. Pavlovvic, S.M. Seraj, An initial investigation of the shape factor platen effects when testing masonry units to determine the material compressive strength, in: Proceedings of the 9th international brick and block masonry conference (IB2MaC), 1991, pp. 653–661.
[48] G. Schickert, Formfaktoren der Betondruckfestigkeit, Die Bautechnik, n.2 58 (1981) 52–57.
[49] A.M. Neville, Properties of Concrete, Pearson Education Limited, 2011.
[50] European Committee for Standardization (CEN), "EN 772-16 Methods of test for masonry units - Part 16: Determination of dimensions." 2011.
[51] European Committee for Standardization (CEN), "EN 772-13 Methods of test for masonry units. Part 13: Determination of net and gross dry density of masonry units (except for natural stone)." 2001.
[52] European Committee for Standardization (CEN), "EN 772-3 Methods of test for masonry units. Part 3: Determination of net volume and percentage of voids of clay masonry units by hydrostatic weighing." 1999.
[53] European Committee for Standardization (CEN), "EN 772-21 Methods of test for masonry units. Part 21: Determination of water absorption of clay and calcium silicate masonry units by cold water absortion." 2011.
[54] N. Makoond, A. Cabané, L. Pelà, C. Molins, Relationship between the static and dynamic elastic modulus of brick masonry constituents, Constr. Build. Mater. 259 (Oct. 2020), 120386, https://doi.org/10.1016/j.conbuildmat.2020.120386.
[55] P. B. Lourenço, J. C. Almeida, and J. A. Barros, "Experimental Investigation of Bricks Under Uniaxial Tensile Testing," J. Br. Mason. Soc. Mason. Int., 18(1) 2005.
[56] European Committee for Standardization (CEN), "EN 998-2 Specification for mortar for masonry. Part 2: Masonry mortar." 2018.
[57] European Committee for Standardization (CEN), "EN 1015-11: Methods of test for mortar for masonry - Part 11: Determination of flexural and compressive strength of hardened mortar." 1999.
[58] COMET, "Coupled Mechanical and Thermal analysis, http://www.cimne.com/comet/," 2016. http://www.cimne.com/comet/.
[59] GiD v.14.0.4, "The personal pre and post-processor, http://www.gidhome.com/," 2020. http://www.gidhome.com/.
[60] R. Faria, J. Oliver, M. Cervera, A strain-based plastic viscous-damage model for massive concrete structures, Int. J. Solids Struct. 35 (14) (1998) 1533–1558, https://doi.org/10.1016/S0020-7683(97)00119-4.
[61] M. Petracca, L. Pelà, R. Rossi, S. Oller, G. Camata, E. Spacone, Regularization of first order computational homogenization for multiscale analysis of masonry structures, Comput. Mech. 57 (2) (2016) 257–276, https://doi.org/10.1007/s00466-015-1230-6.
[62] J. Lubliner, J. Oliver, S. Oller, E. Oñate, A plastic-damage model for concrete, Int. J. Solids Struct. 25 (3) (1989) 299–326, https://doi.org/10.1016/0020-7683(89)90050-4.
[63] L. Pelà, S. Saloustros, P. Roca, Cylindrical samples of brick masonry with aerial lime mortar under compression: experimental and numerical study, Constr. Build. Mater. 227 (2019) 1167–1182, https://doi.org/10.1016/j.conbuildmat.2019.116782.
[64] M. Angelillo, P. B. Lourenço, and G. Milani, "Masonry behaviour and modelling," in: Mechanics of masonry structures, vol. 551, no. January, 2014.
[65] S. Saloustros, M. Cervera, L. Pelà, Tracking multi-directional intersecting cracks in numerical modelling of masonry shear walls under cyclic loading, Meccanica 53 (7) (2018) 1757–1776, https://doi.org/10.1007/s11012-017-0712-3.